https://doi.org/10.1038/s44304-026-00225-4

Inequities in the impacts of compound precipitation extremes on global transportation infrastructures in the late 21st century

Check for updates

Feng Wang[1,2,9], Junhong Guo[3,9], Yurui Fan[4] ✉, Guohe Huang[2,5], YongPing Li[2], Zhenyao Shen[2], Ya Zhou[6], Yizhuo Wen[7] & Amir AghaKouchak[8]

The impact of compound climate extremes on transportation infrastructure is destructive and long-lasting, yet it remains unclear whether these impacts are equitably distributed across countries with different income levels. This study assesses global inequalities in exposure to compound precipitation extremes (CPEs), defined as the concurrent occurrence of short-duration, high-intensity 1-day precipitation (RX1D) and prolonged 5-day precipitation (RX5D), in the late 21st century under multiple climate scenarios. Under SSP585, approximately two-thirds of global transportation infrastructure is projected to experience increased exposure, affecting about 12.6 million km, with at least a 25% reduction in joint return periods, indicating more frequent extremes. Most exposed assets are concentrated in the Global North (10.9 vs. 1.3 million km in the Global South), with the largest absolute exposure in high-income regions (4.9 vs. 0.6 million km in lower-income regions). In contrast, adaptation needs show a clear inverse income gradient. Low-income countries require the highest safety factors (mean 1.31 for 50-year events), followed by lower-middle (1.20), upper-middle (1.17), and high-income (1.15) countries. This pattern remains robust across scenarios and infrastructure types (except motorways), revealing systematic inequality and underscoring the need for income-sensitive adaptation strategies in future infrastructure planning.

Transport infrastructure is essential for the well-functioning of economies and global supply chains[1]. However, in recent years, extreme climate events have severely impacted global transportation infrastructure[2], causing significant economic losses[3]. For example, in 2017, Hurricane Harvey swept through the United States, damaging over 13,000 kilometers of roads in Texas, with repair costs reaching $1.25 billion[4]. In 2019, several European countries experienced severe flooding, resulting in infrastructure losses exceeding €2 billion in Germany alone[5]. Globally, the multi-hazard risk due to direct damage to road and railway assets is estimated to range from 3.1 to 22 billion US dollars, of which ~73% is caused by surface and river flooding[2]. Such damage is expected to increase several-fold over the 21st century because of climate change and the expansion of infrastructure assets[6]. To mitigate the economic and social consequences of natural disasters, the international community, through Sustainable Development Goal (SDG) 9 emphasizes the need to build and maintain resilient, sustainable, and reliable infrastructure[7]. In addition, conducting in-depth research on the impacts of extreme climate events on transportation assets is crucial for developing a climate-resilient and sustainable transportation infrastructure system[2]. This entails identifying high-risk areas, quantifying potential losses under various climate scenarios[8], and formulating adaptive construction and

[1]State Key Laboratory of Earth Surface Processes and Resource Ecology, Faculty of Geographical Science, Beijing Normal University, Beijing, China. [2]Center for Energy, Environment and Ecology Research, UR-BNU, Beijing Normal University, Beijing, China. [3]MOE Key Laboratory of Resource and Environmental, System Optimization, College of Environmental Science and Engineering, North China Electric Power University, Beijing, China. [4]Department of Engineering, Brunel University of London, Uxbridge, Middlesex, United Kingdom. [5]Institute for Energy, Environment and Sustainable Communities, University of Regina, Regina, Saskatchewan, Canada. [6]School of Systems Science, Beijing Normal University, Beijing, China. [7]Key Laboratory of Urban Environment and Health, Institute of Urban Environment, Chinese Academy of Sciences, Xiamen, China. [8]Department of Civil and Environmental Engineering, University of California, Irvine, CA, USA. [9]These authors contributed equally: Feng Wang, Junhong Guo. ✉e-mail: yurui.fan@brunel.ac.uk

management strategies. By enhancing infrastructure resilience, these efforts can help minimize the economic and social losses associated with future extreme events.

Previously, several studies have assessed the direct and indirect impacts of natural disasters on infrastructure networks, including floods[9,10], extreme precipitation[11], wildfires[12], sea level rise[13], earthquakes[14], and extreme wind events[15]. With the intensification of global climate change, transportation infrastructure worldwide has become increasingly exposed to natural hazards[16]. Traditional climate impact studies often analyze individual extremes in isolation. However, real-world infrastructure disruptions are rarely caused by a single extreme event but rather by the interplay of multiple events. Recent studies indicate that many climate-related damages often arise from the compound effects of multiple extreme climate events occurring simultaneously, which can lead to significantly greater impacts than those caused by individual events alone[11]. These occurrences are known as compound extreme events (CEs)[17]. For example, the simultaneous occurrence of high temperatures, drought conditions, high fuel loads, and strong winds leads to an increased fire danger in eastern Australia during 2019–2020[18]. Intense rainfall combined with storm surges can lead to widespread flooding, overwhelming drainage systems and causing severe disruptions to transportation networks[19]. Although many climate-related damages of transport infrastructure are caused by compound events, the understanding, analysis, quantification and prediction of such events are still in their infancy[17]. As climate change increases the frequency and intensity of CEs, understanding their combined impacts is crucial for improving risk assessments and developing effective adaptation strategies.

Among various CEs, this study focuses on the impacts of compound precipitation events (CPEs) on transportation infrastructure, defined as the simultaneous occurrence of 1-day (RX1D) and 5-day (RX5D) extreme precipitation. RX1D represents short-duration, high-intensity rainfall events that often trigger flash floods and urban inundation, while RX5D captures prolonged precipitation periods that lead to soil saturation and sustained riverine flooding[20]. Although RX5D mathematically aggregates daily precipitation and therefore may include extreme daily amounts, the two indices characterize distinct physical dimensions of rainfall extremes—namely intensity and persistence[18,20]. In this study, we use the term "compound" to describe events in which extreme short-term intensity occurs within an already extreme multi-day accumulation period. Such CPEs reflect the joint manifestation of peak rainfall intensity and prolonged moisture input, rather than a single-duration extreme.

Physically, these events may arise from persistent large-scale circulation systems (e.g., quasi-stationary fronts or tropical cyclones) that generate multi-day rainfall, within which embedded convective bursts produce extreme daily totals. From a hydrological perspective, prolonged rainfall increases soil moisture and reduces infiltration capacity. When extreme short-duration rainfall occurs over already saturated terrain, runoff generation efficiency increases substantially, potentially escalating flood risks and causing severe disruptions to transportation infrastructure[21]. Such intensity–persistence compounding effects can increase damage to roads, railways, and bridges, resulting in higher maintenance costs and prolonged service interruptions. However, quantitative assessments of these compound precipitation impacts remain limited. The co-occurrence of these two extremes is hypothesized to produce non-linear and amplified impacts that exceed the sum of their individual effects. Specifically, when extreme short-duration rainfall occurs over already saturated terrain due to prior prolonged precipitation, flood risks can escalate dramatically, leading to severe disruptions to transportation infrastructure. Such compounding effects can increase damage to roads, railways, and bridges, resulting in higher maintenance costs and prolonged service interruptions.

Despite numerous studies examining the effects of climate extremes and associated natural hazards on transportation systems (as well as the resultant risk of transportation-system failure), most have been limited to single-duration precipitation extremes at regional scales[10,22,23]. There is a lack of research on the projected global impacts of CPEs in terms of both intensity and duration over the upcoming century. On the other hand, developed countries have generally emitted more greenhouse gases (GHGs) and are therefore more responsible for the intensification of compound extremes; however, the impacts of such extremes on transportation infrastructure in developing countries are often more severe. This raises a major issue of equity among countries worldwide. However, no study has systematically examined this issue. Such research is crucial for developing effective strategies aimed at reducing poverty (SDG 1) and global inequality (SDG 10), increasing access to sustainable transport infrastructure in low- and middle-income countries, and combating the impacts of climate change (SDG 13)[7].

Therefore, our study aims to reveal inequalities arising from the differentiated impacts of CPEs under climate change on global transportation infrastructure in the late 21st century; such CPEs are characterized based on projections of annual maximum one- and five-day precipitation during 2041–2100. In detail, this objective entails the following contributions: First, we will identify annual maximum one- and five-day precipitation intensities for 2041–2100 through Copula analysis and non-linear optimization, providing insights into the interactions among intensity, duration, and frequency of precipitation extremes over extended periods. Second, based on projected CPEs, we will estimate their impacts on transportation infrastructure and the associated risks of system failure, using 11 high-resolution CMIP6 datasets; such risks will be quantified through the analyses of uncertainties in both CPEs (under changing climatic conditions) and transportation-infrastructure conditions. Third, we will develop adaptation measures across countries with different income levels based on a proposed safety factor (defined as the ratio of future to historical extremes). The proposed safety factors will enable: 1) translating the projected high-resolution (temporally and spatially) CPEs into "actionable" information as required by policy makers and practitioners, and 2) improving the related infrastructure codes (e.g., highway codes, bridge codes) to adapt to climate-change impacts in the upcoming century. Finally, we will provide a global data portal of grid-scale (0.25° × 0.25°) safety factors, facilitating the transfer of our methods and findings to policymakers and practitioners.

Results

Spatial variability in projected CPEs and infrastructure exposure

The joint return periods (JRPs) of the most-likely CPEs with a 50-year or 100-year JRP during 1951–2010 were projected for the future period (2041–2100) under different climate change scenarios. Specifically, the most-likely precipitation magnitudes of RX1D and RX5D associated with the historical 1-in-50-year or 1-in-100-year CPEs were calculated for all grids using the copula models fitted to the historical CPE series. Subsequently, for each grid, the future JRPs corresponding to these historical CPE magnitudes were estimated using copula models constructed from future CPE series, thereby revealing how the risk of CPEs may evolve under climate change. A detailed description of the methodological framework is provided in the Methods section. Figure 1a, b shows the projected future JRPs (2041–2100) of the historical 50-year and 100-year CPEs under the SSP585 scenario. The results for other scenarios (SSP126, SSP245, and SSP370), along with their associated uncertainties, are presented in Supplementary Figs. S1, S2.

Figure 1a, b shows that CPEs are projected to increase globally on average. However, the magnitude and direction of these changes exhibit pronounced regional heterogeneity, with some areas experiencing little change or even decreases in frequency (Fig. 1; Supplementary Table S1). Under the SSP585 scenario, ~76.9% (72.1%) of global land areas are projected to experience reduced JRPs for the historical 50-year (100-year) CPEs as a consequence of global warming. Specifically, for the historical 1-in-50-year CPEs, it is projected that 49.8% of global regions will experience a decrease in JRPs by more than 50%, implying that these events may occur more frequently than once every 25 years in the future. In alignment with this trend, it is estimated that 49.4% of the world will see historical 100-year CPEs transition to events occurring every 50 years or even more frequently in the future. From a continental perspective (Supplementary Table S1), it is evident that 83.2% of North America will experience increased CPEs in the

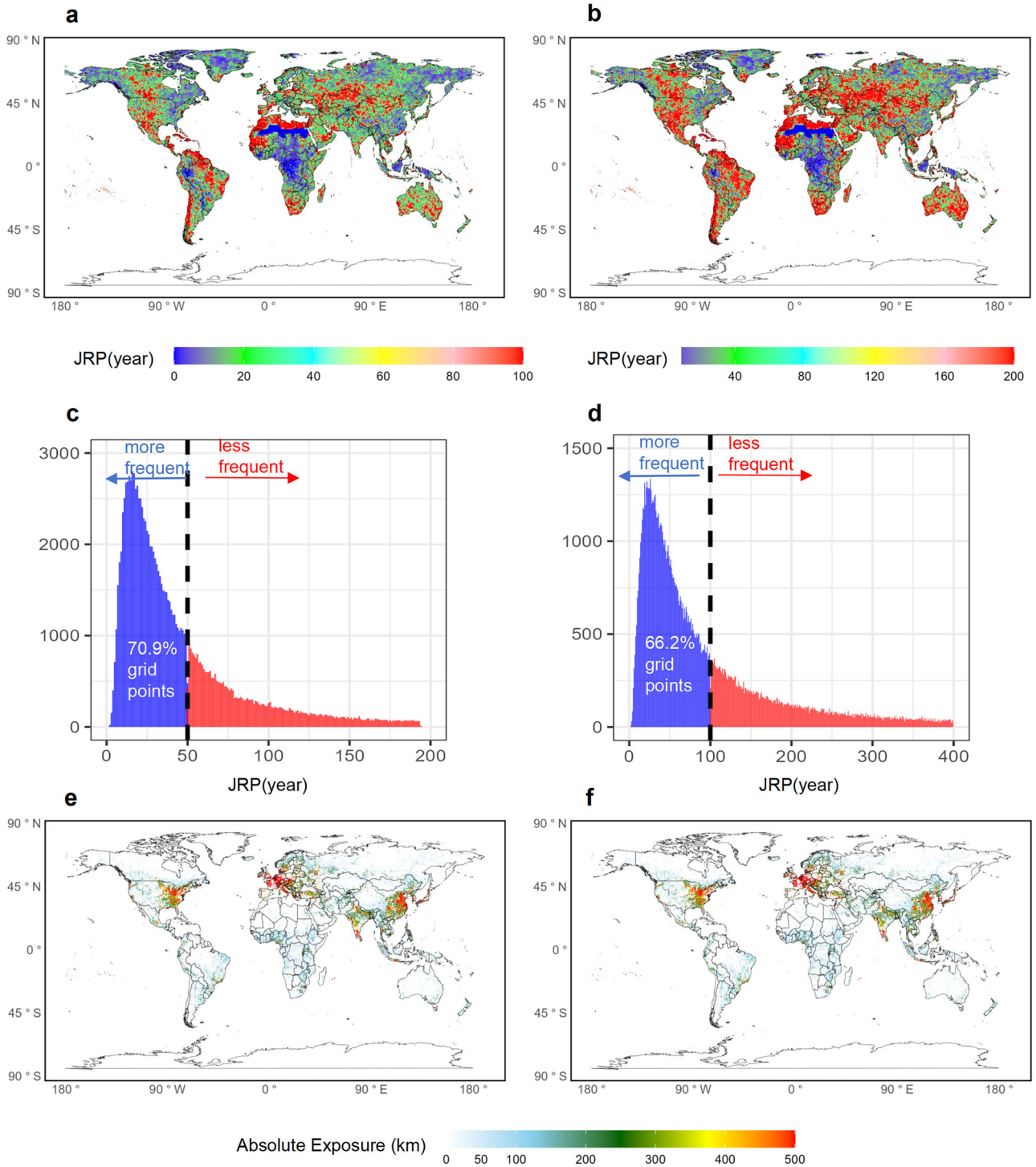


Fig. 1 | Future changes in Compound Precipitation Extremes (CPEs) and associated exposure risks for global transportation infrastructure. a, **b** Projected joint return period (JRP) during 2041–2100 of historical (1951–2010) most-likely CPEs under SSP585 scenario (**a** historical 50-year CPEs, and **b** historical 100-year CPEs). **c**, **d** Distribution of global road and railway assets exposed to changes in JRP (years) under the SSP585 scenario (**c** historical 50-year CPEs, and **d** historical 100-year CPEs). Red and blue colors denote the transportation assets exposed to less frequent and more frequent CPEs, respectively. **e**, **f** Spatial distribution of the absolute exposure of global road and railway assets under the SSP585 scenario (**e** historical 50-year CPEs, and **f** 100-year CPEs). Results are presented at a spatial resolution of 0.25° × 0.25°. Absolute exposure is defined as the total length of road and railway assets within each cell that is subjected to a decrease of more than 25% in the future JRPs relative to the historical baseline.

future, followed by Asia (80.4%), Africa (76.8%), Oceania (74.0%), Europe (70.3%), South America (63.1%), and Australia (52.1%). Notably, East Asia, Central Africa, Eastern Europe, and Greenland are identified as hotspot regions particularly vulnerable to global warming, experiencing substantial shortening of JRPs for historical 50-year and 100-year CPEs. Conversely, some regions such as North Africa, Central Asia, southern Europe, and central North America may also see increased JRPs (indicating a decreased frequency) of severe CPEs. This suggests that these regions might experience region-specific shifts in precipitation variability, with potential implications for hydrological extremes. Notably, the pronounced shortening of JRPs in

high-latitude regions such as Greenland does not necessarily imply exceptionally large absolute precipitation amounts. Instead, it reflects substantial relative increases in extreme precipitation compared to historically low baseline conditions. Continental-scale statistics (Supplementary Table S2) show that high-latitude regions experience consistent increases in both RX1D and RX5D under future scenarios. Because joint return periods are sensitive to upper-tail distribution shifts, even moderate absolute increases can substantially elevate the exceedance probability of historical extreme thresholds. Consequently, regions with relatively low historical precipitation may exhibit disproportionately large percentage changes in CPE frequency under warming.

Figure 1c, d display the global distribution of road and railway assets undergoing changes in JRPs in the future under the SSP585 scenario. The results for other scenarios (SSP126, SSP245, and SSP370) are shown in Supplementary Fig. S3. Our results reveal that approximately two-thirds of global transportation infrastructure will face increased exposure to CPEs. Specifically, about 70.9% of global transportation assets are expected to experience more frequent CPEs that historically occurred once every 50 years, with the average recurrence interval shortening to ~24 years in the future. Similarly, around 66.2% of global transportation assets are projected to be exposed to historical 100-year CPEs at a substantially higher frequency, occurring on average once every 45 years. More specifically, over three-quarters of transportation assets in Asia (76.8%) and Africa (76.2%) are projected to experience increased occurrences of historical 50-year CPEs, while the majority of transportation assets in Oceania (69.9%), North America (67.6%), Europe (66.1%), and South America (64.3%) are also expected to face these CPEs more frequently in the future. However, approximately half of the assets in Australia (49.0%) are projected to experience an increase in CPE occurrences, primarily because the less-affected regions (52.7%) are expected to encounter more frequent CPEs. A similar pattern is observed for historical 1-in-100-year CPEs, as shown in Supplementary Table S3. However, as evidenced by Supplementary Tables S1, S2, climate change mitigation strategies can significantly reduce the likelihood of CPE events and their associated threats to future transportation infrastructure. The proportion of land experiencing increased frequency of historical 50-year CPEs is projected to decline from 76.9% under SSP585 to 57.0% under SSP126, while the percentage of global transportation assets facing these more frequent CPEs is correspondingly reduced from 70.9% to 51.9%.

The absolute exposure of infrastructure assets to CPEs is jointly determined by two factors: the spatial distribution of the assets and the change in the design return period at a given location[8]. The spatial distribution of the absolute exposure of worldwide transportation infrastructure to CPEs under the SSP585 scenario is depicted in Fig. 1e, f. This absolute exposure is calculated by aggregating all road and railway assets within a grid of 0.25° × 0.25° that experience a future reduction of more than 25% in the JRP of the corresponding CPE (see Methods). We find that, by the late twenty-first century, 12.2 million km of global road and railway assets will be exposed to significantly more frequent historical 50-year CPEs (i.e., a JRP reduction exceeding 25%), representing 52.5% of the global land transport infrastructure. The absolute exposure also exhibits pronounced regional disparities, with the Global North experiencing more than eight times the exposure of the Global South (e.g., 10.9 versus 1.3 million km for JRP50 under SSP585). Regions with substantial absolute exposure are concentrated in the eastern part of North America, much of Europe, South Asia, and East Asia, largely reflecting the dense transportation networks in these areas. At the same time, 11.4 million km of transport infrastructure assets are projected to be exposed to historical 100-year CPEs with JRPs further reduced by more than 25%. The spatial distribution of absolute exposure to historical 100-year CPEs closely mirrors that observed for historical 50-year CPEs.

The spatial distributions of absolute exposure under the SSP126, SSP245, and SSP370 scenarios are illustrated in Supplementary Fig. S4. Under these scenarios, the length of exposed transportation assets will respectively decrease to 7.7, 9.7, and 10.9 million km in absolute exposure to the historical 50-year CPEs. Correspondingly, the absolute exposure of transportation assets to historical 100-year CPEs will decrease to 7.0, 8.8, and 10.1 million km, respectively. These results suggest that greenhouse gas emission reductions and climate change mitigation strategies can significantly reduce the impact of extreme rainfall on transportation facilities. Furthermore, the regional disparities remain consistent across different SSP emission scenarios and varying levels of CPE severity. The percentages of absolute exposure for the six types of road and railway assets under the four SSP scenarios in the future are presented in Supplementary Table S4. The results indicate that the absolute exposure percentages of different transportation facilities exhibit similar patterns, with motorways showing the highest absolute exposure levels.

Unequal transportation exposure for different income country groupings

Figure 2a–c shows the top 20 countries with the longest total lengths and absolute exposure lengths of infrastructure assets under the SSP585 scenario. The country rankings under the SSP126, SSP245 and SSP370 scenarios can be found in Supplementary Fig. S5. In detail, China (CHN) has the longest absolute exposure length, primarily due to its densely distributed transportation infrastructure (ranked second in total length) and increased frequencies of CPEs, particularly along the east coast. Moreover, about 66.6% of land areas in China, as shown in Fig. 1a, are projected to experience more frequent occurrences of historical 50-year CPEs (i.e., a 25% reduction in future JRP) in the late 21st century. Notably, the length of transportation assets in China exposed to these events is projected to reach 2.23 million km, accounting for 81.4% of the country's total transportation network (Figs. 1e and 2b). For historical 100-year CPEs, the corresponding proportions are expected to be 60.3% for land areas and 71.4% (2.14 million km) for transportation assets. These findings imply that China's transportation infrastructure is disproportionately concentrated in regions projected to experience substantially more frequent CPEs in the future.

Although the US has the longest total length of transportation assets and the second longest length of absolute exposures to CPEs, the spatial distributions of CPEs and absolute exposures of transportation assets differ markedly from those observed in China. In the late 21st century, 59.6% of US land areas are projected to face significantly more frequent occurrences of historical 50-year CPEs, yet only 60.5% (2.14 million km) of its transportation assets are located in these areas. For historical 100-year CPEs, the proportion of affected land areas is estimated at 55.0%, while the proportion of transportation assets exposed declines to 47.4% (1.67 million km). These findings suggests that, despite the extensive scale of US transportation infrastructure, it is relatively less concentrated in regions projected to face heightened CPE risk, indicating a more geographically dispersed network and comparatively greater resilience to future CPEs.

The countries featured in the top 20 with the greatest absolute exposures to historical 50-year (Fig. 2b) largely overlapped (19 countries in common) with those to 100-year CPEs (Fig. 2c), including a total of 9 high income (HI), 7 upper middle income (UMI), and 3 lower middle income (LMI) countries. Notably, the top four countries experiencing the longest absolute exposure to historical 50-year and 100-year CPEs remain consistent: China (CHN), the United States (USA), Russia (RUS), and India (IND). However, clear differences emerge between country rankings in total infrastructure length and absolute exposures to CPEs, underscoring a nuanced interplay between infrastructure density and climate change impacts. For instance, Australia (AUS) and Sweden (SWE) rank, respectively, 11th and 20th in terms of total infrastructure length. Under the SSP585 scenario, their rankings for absolute exposure to historical 100-year CPEs shift to 19th for AUS and 11th for SWE. This divergence indicates that infrastructure exposure and resilience are not determined solely by network size but are also strongly influenced by climatic factors, particularly shifts in precipitation regimes. Understanding these dynamics is critical for developing comprehensive strategies that address the multifaceted challenges associated with infrastructure vulnerability on a global scale.

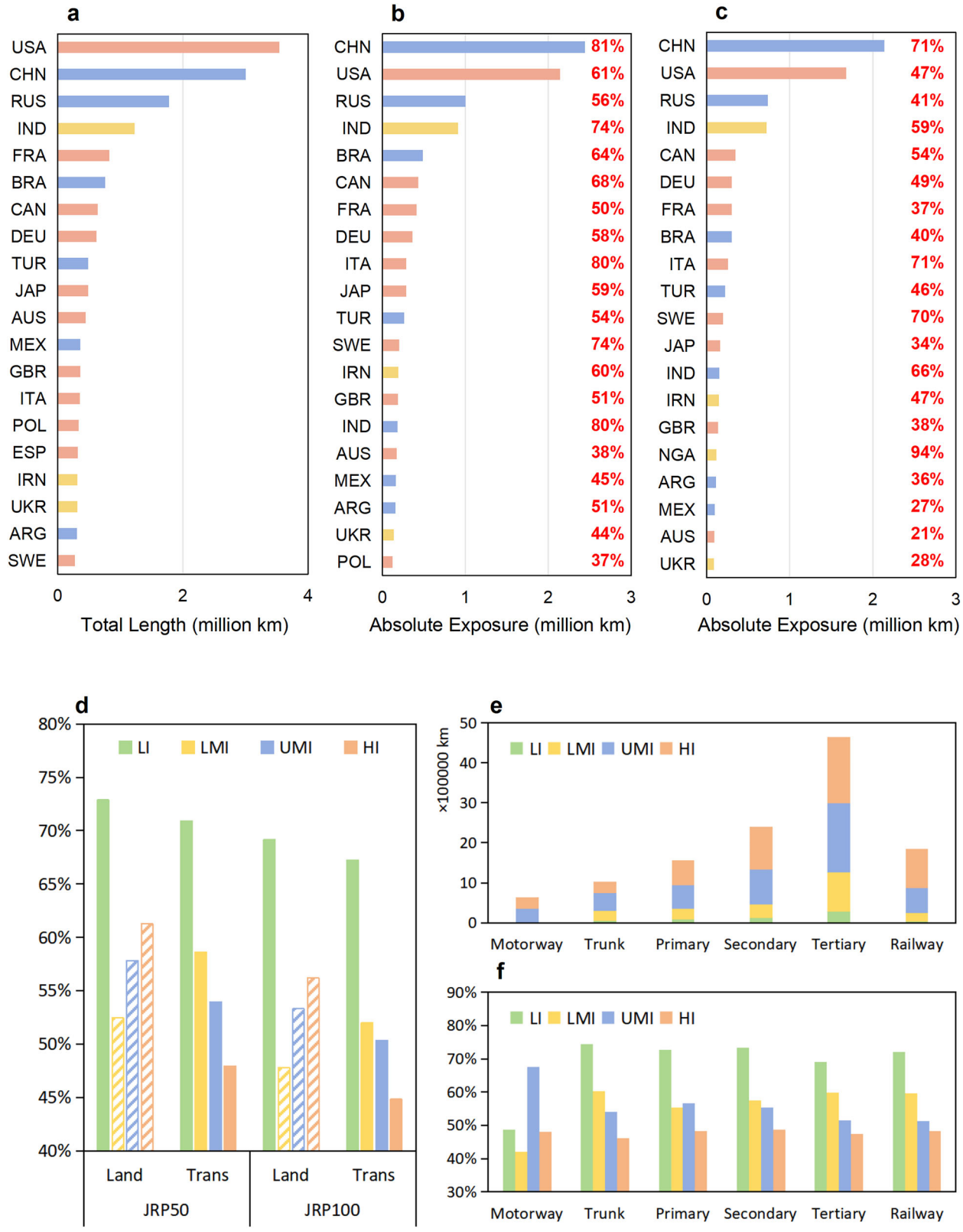


Figure 2d illustrates the proportions of land areas and transportation assets exposed to historical 50-year and 100-year CPEs undergoing a reduction of more than 25% in future JRPs, across different country income groups under SSP585. These exposure rates vary markedly by income level. Specifically, low-income (LI) countries exhibit the highest exposure rates, with ~72.9% and 69.1% of land areas for historical 50-year and 100-year CPEs respectively, and 70.9% and 67.2% of transportation assets, respectively (as shown in Supplementary Table S6). These findings highlight the disproportionate vulnerability of LI countries to future climate extremes. In lower-middle-income (LMI) countries, ~52.5% of land areas are projected to experience significantly increased occurrences of historical 50-year CPEs (with a 25% reduction in future JRP). Additionally, 58.6% of the

Fig. 2 | Transportation exposure across different income country groupings. **a**–**c** Country rankings by total transportation assets length and absolute exposure to historical 50-year and 100-year CPE events. **a** Ranking in total length of transportation assets. **b** Ranking in absolute exposure to historical 50-year CPEs. **c** Ranking in absolute exposure to historical 100-year CPEs. The absolute exposure is defined as the total length of road and railway assets within a grid exposed to CPEs with a reduction of more than 25% in future JRPs. The red percentage values in panels (**b**) and (**c**) indicate relative exposure, representing the proportion of absolute exposure length relative to the total transportation asset length. The abbreviations and corresponding full names of countries are presented in Supplementary Table S5. **d**–**f** Proportions of land areas and transportation assets exposed to more frequent historical CPEs (25% reduction in the future JRP) across different country income groupings in the late 21st century under the SSP585 scenario. **d** displays the proportions of land areas and transportation assets exposed to historical 50-year and 100-year CPEs. **e** And **f** present detailed information on the total length and corresponding proportions of six specific types of transportation assets exposed to historical 50-year CPEs. "LI" refers to low-income countries, "LMI" to lower-middle-income countries, "UMI" to upper-middle-income countries, and "HI" to high-income countries.

transportation assets in LMI countries are projected to be exposed to these events, indicating a pronounced concentration of infrastructure in high-risk areas. A similar pattern is expected for historical 100-year CPEs. In contrast, high-income (HI) countries, although most areas are projected to experience significant increases in CPE occurrences (e.g., 61.3% for historical 50-year CPEs), their transportation assets (47.9% for historical 50-year CPEs) are less concentrated in those affected areas. A comparable pattern is observed in upper-middle-income (UMI) countries, where transportation infrastructure is relatively less concentrated in high-risk zones. These findings highlight the urgent need for targeted adaptation and resilience measures, especially in low-income (LI) and lower-middle-income (LMI) countries, to mitigate the impacts of climate change on infrastructure, communities, and economic activities. Such measures could include infrastructure upgrades, improved land use planning, and capacity building to enhance resilience and reduce vulnerability to future climate-related extreme events.

Transportation infrastructure comprises multiple asset types—including railways, motorways, trunk roads, primary roads, secondary roads, and tertiary roads—which exhibit heterogeneous exposure patterns across income groups. Figure 2e, f presents the absolute exposure lengths and corresponding proportions for six asset categories under SSP585. Although UMI and HI countries have longer total exposed road lengths, LI and LMI countries display higher exposure proportions across nearly all asset categories (except motorways). Specifically, in LI countries, all road types except motorways are projected to experience exposure proportions exceeding 70%, representing the highest levels among all income groups. Motorways in LI countries, while not the most exposed category, still exhibit the second-highest exposure proportion overall. This pattern highlights the particularly elevated vulnerability of transportation systems in LI countries to future climate change impacts. Notably, in LMI countries, the exposure proportions of all road types except motorways are projected to range from 55.4% to 60.3%, exceeding the corresponding land exposure proportion (52.2%). These results further emphasize that the infrastructure in LMI countries is more concentrated in areas significantly affected by future CPEs. Conversely, HI countries exhibit a different trend, with all road types showing exposure proportions ranging from 46.1% to 48.7%, which are lower than those of land areas at 61.3%. Similar patterns are observed in UMI countries. These results suggest comparatively greater resilience in the distribution of transportation infrastructure within higher-income countries. Nevertheless, motorways in UMI countries stand out, with the longest absolute length (0.32 million km) of absolute exposure and also the highest exposure proportion (67.5%), which is significantly higher than the that of land areas (57.8%). This indicates a substantial threat of future CPEs on motorways in UMI countries.

Supplementary Table S6 presents the proportions of absolute exposure to different historical CPEs across land areas and transportation assets for various country income groups under four SSP scenarios. When comparing the SSP585 and SSP126 scenarios, the exposure proportions of land and transportation to historical 50-year and 100-year CPEs are consistently lower under SSP126 across countries with different income levels. Specifically, taking historical 50-year CPEs as an example, LI countries exhibit the most pronounced differences, with land and transportation exposure being 25% and 23% lower, respectively, under SSP126. In contrast, HI countries show the smallest reduction, with land and transportation exposures being 22% and 16% lower, respectvely. Even so, only 39.6% of land areas and 31.7% of transportation assets in these countries are projected to experience absolute exposure to these CPEs. This suggests that adopting a more sustainable development pathway can effectively enhance the resilience of transportation assets to climate extremes across countries of different income levels. This is particularly crucial for LI and LMI countries, where transportation assets are more vulnerable to future CPEs. Implementing sustainable development pathways not only reduces the risk associated with CPEs but also supports the long-term stability and adaptive capacity of transportation infrastructure in coping with such extremes.

Safety factor analysis for climate change adaptation

The majority of transportation infrastructure is planned and constructed under the assumption that precipitation patterns will remain consistent with historical records. However, changes in precipitation regimes associated with global warming are likely to increase the vulnerability of infrastructure assets in many regions worldwide. To address this issue, Liu et al.[8] recommend incorporating a climate change adaptation safety factor (see Methods) when upgrading existing infrastructure or designing new projects. This safety factor aims to ensure that the infrastructure maintains an acceptable level of risk under future warming scenarios. Accordingly, the safety factor required for transportation infrastructure to adapt to climate change with respect to CPEs is defined as the ratio of the sum of the future most-likely RX1D and RX5D values to the sum of their corresponding historical values under identical return periods (JRP). A larger safety factor indicates that future CPEs are projected to be more intense, implying greater potential risks to transportation infrastructure and the need for additional measures or interventions to enhance resilience against such CPEs. The detailed calculation procedure is provided in the Methods section.

Figure 3 illustrates the spatial distribution of safety factors for transportation infrastructure, focusing on adaptation to 50-year CPEs under the SSP585 scenario. In the majority of regions (over 95.5%), transportation assets require enhanced resilience, as indicated by safety factors greater than 1. Specifically, as shown in Supplementary Table S7, ~45.6% of land areas will need a safety factor in the range of 1.0–1.2 to adapt to 50-year CPEs in the late 21st century, while 57.7% of current transportation assets are located in these areas. Meanwhile, another 41.9% of global regions, hosting 32.6% of transportation assets, require a safety factor in the range of 1.2–1.4 for the same purpose. Moreover, a small proportion of land areas (8.0%) and transportation assets (3.1%) require substantial resilience enhancement, with safety factors exceeding 1.4; these areas are primarily concentrated in Tibet, Central Africa, and the Andes in South America. Under the SSP126 scenario, the majority of land areas (71.4%) and transportation assets (75.8%) require a safety factor in the range of 1.0–1.2 to adapt to 50-year CPEs in the late 21st century. Additionally, ~21.6% of land areas and 14.6% of global transportation infrastructure exhibit safety factors between 1.2 and 1.4. Only a small fraction of land areas (1.5%) and transportation assets (0.7%) require a safety factor exceeding 1.4. For different SSP scenarios, the global mean safety factor for land areas would decreases from 1.21 (SSP585) to 1.19 (SSP370), 1.16 (SSP245), and 1.14 (SSP126), when considering 50-year CPEs (as shown in Supplementary Fig. S6 and Supplementary Table S6). The uncertainty of the required safety factor under different SSP scenarios is presented in Supplementary Fig. S7. The safety factor exhibits different levels of uncertainty across SSP scenarios. Under SSP245, uncertainty is lowest (global mean: 0.47 for 50-year

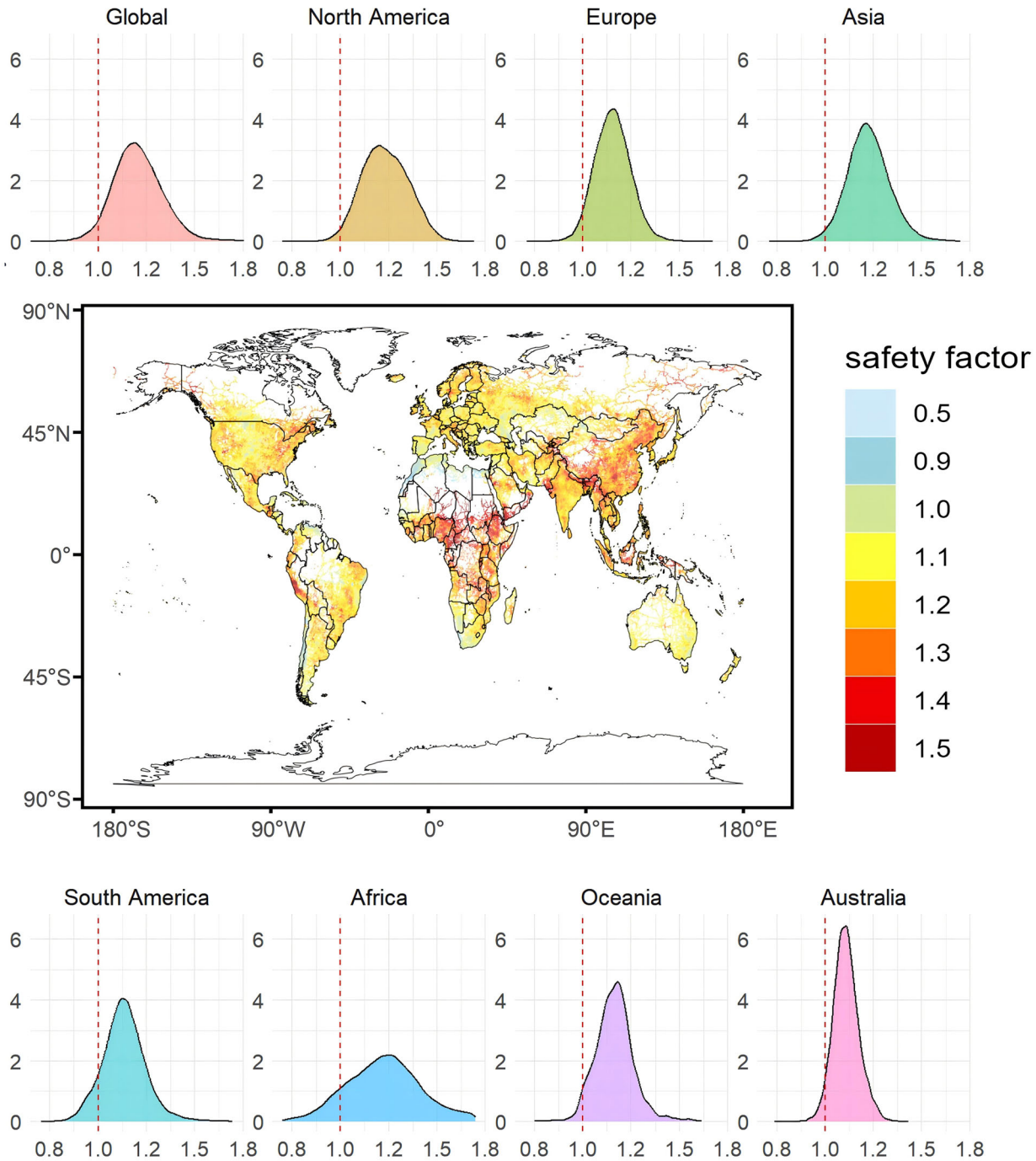


Fig. 3 | Spatial distribution of the required safety factors for transportation infrastructure, aimed at climate change adaptation to 50-year CPEs under the SSP585 scenario. Results are shown in a grid resolution of ~25 km × 25 km. A value of 1 indicates no changes in the CPEs, while a value larger 1 means resilience enhancements are required for transportation infrastructure to adapt to future CPEs.

CPEs), indicating higher model consistency and greater predictability of safety factor. In contrast, SSP370 shows the highest uncertainty (global mean: 0.51 for 50-year CPEs), reflecting greater model divergence and lower safety factor predictability. The variability in the required safety factor highlights the importance of climate mitigation measures for enhancing transportation infrastructure resilience. Although climate mitigation measures do not significantly reduce the proportion of land or current infrastructure requiring enhanced resilience, they substantially reduce the required level of resilience, thereby reducing the costs associated with resilience enhancement. Moreover, future climate changes will lead to more intense CPEs in the Northern Hemisphere (Supplementary Tables S8). The average safety factor in the Northern Hemisphere exceeds that in the Southern Hemisphere (e.g., 1.23 versus 1.15 under the SSP585 scenario for 50-year CPEs). As depicted in Supplementary Tables S7, S8, this pattern is consistent across different types of transport facilities (e.g., motorway, trunk, primary, secondary, tertiary, and railway), different SSP scenarios, and different CPEs (e.g., historical 50-year and 100-year CPEs). This result indicates that, under the selected compound precipitation events, transportation assets in the Northern Hemisphere are exposed to relatively higher hazard intensification, as reflected by the larger safety factors required.

Figure 3 further illustrates the distribution of safety factors required for transportation infrastructure adaptation to climate change across continents. The mean safety factor required for transportation facilities is highest in Africa at 1.28, followed by North America (1.23), Asia (1.22), Oceania (1.16), Europe (1.14), South America (1.14), and Australia (1.11). Moreover, the distribution of safety factors required in Africa is the most dispersed, with a maximum variance of 0.22, followed by South America (0.12), Asia (0.11), North America (0.10), Europe (0.09), Oceania (0.09), and Australia (0.07). These results reflect differences in projected compound precipitation intensification and exposure patterns across regions. The relatively higher mean and variance of safety factors in Africa indicate stronger projected hazard amplification and greater spatial heterogeneity under the selected compound precipitation scenarios, suggesting that transportation systems in this region may require comparatively larger design margins under equivalent hazard benchmarks.

Unequal safety factors for different country income groupings

Countries with different income levels exhibit significant differences in the safety factors required for transportation infrastructure resilience to future CPEs (as shown in Fig. 4a). Globally, transportation infrastructure in LI countries needs to be assigned the highest safety factor (1.31), followed by LMI (1.20), UMI (1.17) and HI (1.15) countries, indicating the greater vulnerability of transportation infrastructure in LI and LMI countries to future climate change. Among all transportation infrastructure, trunk roads in LI countries require the highest safety factor (1.32). It is noteworthy that, for motorways, the inequality index is the lowest among all road types, indicating that safety factors are more similar across income groups. This contrasts with other road categories, where low-income countries generally exhibit significantly higher safety factors. An inequality index is used to reflect the variation in safety factors among different income groups, defined as the ratio of variance to mean, with higher values indicating greater disparity As illustrated in Fig. 4a and Supplementary Fig. S8, different types of transportation infrastructure exhibit varying inequality indices. Among them, trunk roads show the highest inequality in required safety factors, with a safety factor of 1.32 required for LI countries compared to 1.15 required for HI countries. In contrast, motorways show a much lower dispersion of safety factors. This is primarily because low-income countries exhibit relatively lower safety factors for motorways compared to other road types, which narrows the gap with higher-income groups. This pattern is closely linked to the extremely limited extent of motorway infrastructure in low-income countries. Motorways account for only 3763 km (~0.5% of total road length) in low-income countries, compared to 479,870 km (5.6%) and 597,648 km (5.8%) in upper-middle- and high-income countries, respectively. Given their scarcity, motorways in low-income countries are typically constructed in strategically important locations and are subject to higher design standards, which may reduce their relative sensitivity to projected hazard intensification. As a result, safety factor requirements are comparatively lower, leading to a more convergent distribution across income groups and a reduced inequality index. For the 100-year CPE, the patterns of safety factors and inequality indices remain consistent with those observed for the 50-year CPE.

To further explore the unequal impacts of CPEs on transportation infrastructure across countries with different income levels, 20 representative countries are selected with five countries from each income group that have the longest total transportation infrastructure length. Figure 4b displays the distribution of safety factors for these 20 representative countries. It can be observed that among these 20 countries, the top three countries with the highest mean safety factors are SDN (1.40), ETH (1.33), and COD (1.31), all of which belong to the low-income group. Meanwhile, the top three countries with the highest variances in safety factors are DZA (0.21), COD (0.13), and SND (0.13), which primarily belong to the low- or lower-middle-income groups. This indicates that transportation infrastructure in LI and LMI countries faces significant challenges in adapting to future climate change, especially under compound precipitation extremes. Our results further suggest that, to address future extreme weather events, particularly compound extreme precipitation, and mitigate disaster risks, LI and LMI countries need to allocate more resources to infrastructure construction and maintenance. This, in turn, places additional financial and technological support burdens on these countries. Moreover, limited resources for resilient infrastructure upgrades, along with other climate-related impacts (e.g., sea level rise) are likely to further exacerbate economic pressures on these nations.

Figure 5 shows the projected changes in safety factors for transportation infrastructure across four income groups under different SSP scenarios. Overall, the required safety factor declines as the scenario shifts from SSP585 to SSP126. The reduction is most pronounced in low-income (LI) countries, decreasing from 1.31 (SSP585) to 1.17 (SSP126). High-income (HI) countries exhibit a smaller but consistent decline, from 1.15 to 1.11. Across all income groups, the largest reduction occurs during the transition from SSP370 to SSP245. The inequality index (variance-to-mean ratio) based on safety factors decreases progressively from 0.06 (SSP585) to 0.02 (SSP126) (Fig. 5b), indicating reduced disparities among income groups under stronger mitigation scenarios. Uncertainty in safety factors, represented by the inter-model variance across 11 CMIP6 models, also varies across scenarios (Fig. 5c). The highest uncertainties are observed under SSP370, particularly for high-income countries. The largest reduction in uncertainty occurs between SSP370 and SSP245. The inequality index based on uncertainty exhibits a non-monotonic pattern, with the lowest value under SSP370 (Fig. 5d), suggesting relatively more homogeneous uncertainty levels across countries under this scenario.

Discussion

The increasing concurrence of RX1D and RX5D reflects the combined influence of thermodynamic and dynamic processes under climate warming. Enhanced atmospheric moisture availability, consistent with the Clausius-Clapeyron relationship, intensifies short-duration precipitation extremes, while alterations in large-scale circulation patterns, moisture transport pathways, and storm persistence contribute to prolonged rainfall accumulation. The joint manifestation of peak intensity and multi-day persistence therefore represents not merely a statistical aggregation, but a physically plausible outcome of a warming climate system. Importantly, the hydrological impacts of such compound events are inherently nonlinear: extreme daily rainfall occurring over already saturated soils substantially increases runoff efficiency and flood potential. Therefore, assessing RX1D and RX5D jointly is necessary to capture escalation mechanisms that cannot be fully represented by single-duration metrics. This intensity-persistence framework provides a more impact-relevant characterization of precipitation extremes for infrastructure risk assessment.

Our results indicate that projected changes in compound precipitation extremes translate into spatially heterogeneous exposure patterns for global transportation infrastructure. Because transportation networks are unevenly distributed across climatic zones, the interaction between hazard intensification and infrastructure density generates regionally differentiated exposure burdens. Areas with dense infrastructure and increasing compound hazard frequency experience disproportionate exposure growth, whereas regions with sparse networks may show lower absolute exposure despite substantial hazard shifts. This spatial mismatch between hazard amplification and infrastructure concentration underlies the observed cross-regional inequalities. Notably, LI countries exhibit higher proportions of infrastructure located in areas subject to intensified compound extremes, suggesting that exposure inequality arises not solely from hazard intensification but also from structural development patterns. The unequal distribution of exposure therefore reflects the coupling of climate dynamics with historical infrastructure expansion trajectories.

Beyond exposure, the required safety factors reveal systematic disparities in adaptation needs across income groups. Higher safety factors in low- and lower-middle-income countries indicate that projected hazard intensification, under standardized return-period benchmarks, would necessitate relatively larger design margins to maintain equivalent protection levels. As the safety factor is defined as the ratio between future and

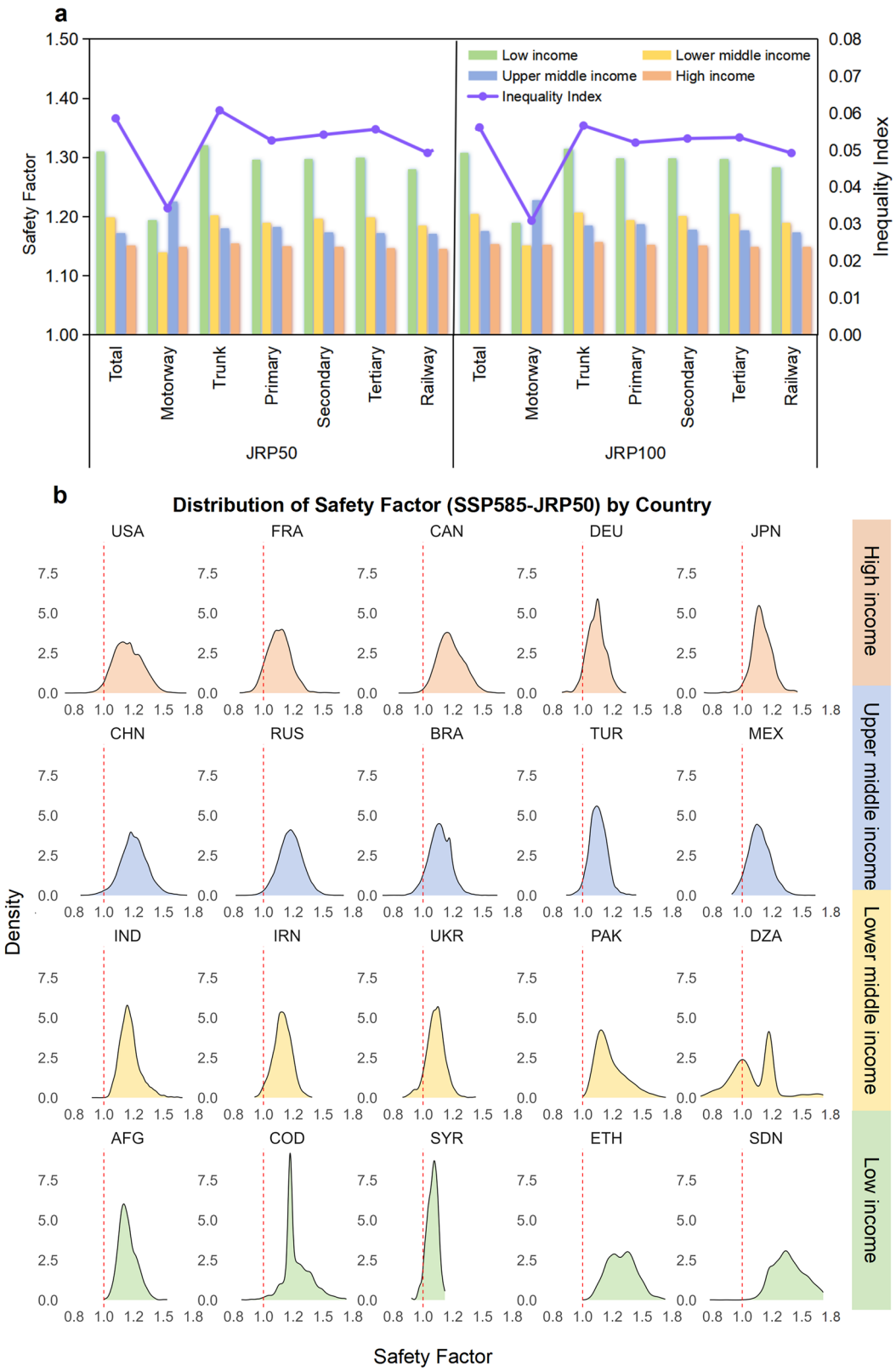


Fig. 4 | Safety factors for different country income groupings. a Safety factor of transportation infrastructure for different country income groupings. **b** Safety factor distributions for climate change adaptation for representative countries in different income groups.

historical compound precipitation extremes under the same joint return period and is computed at the grid level before aggregation, its spatial variation primarily reflects the spatial heterogeneity and intensification of hazards, rather than the distribution of infrastructure itself. By contrast, inequalities in exposure metrics arise from a combination of hazard intensification and the spatial distribution of infrastructure. Absolute exposure, measured as the total length of affected transportation assets, is inherently influenced by where infrastructure is located, and thus reflects the interaction between hazard changes and existing network layouts. To better isolate the role of hazard-driven changes, we further examine relative

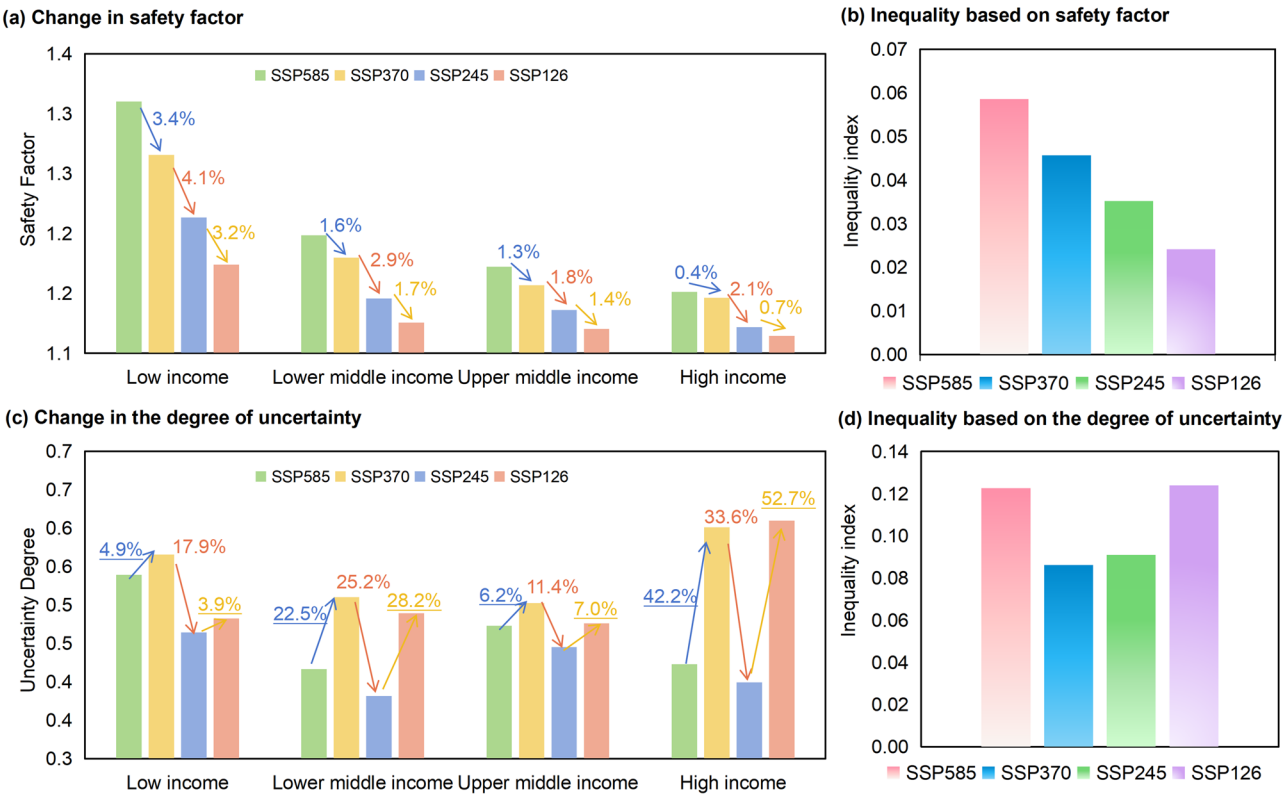


Fig. 5 | Safety factors and their uncertainties for transportation infrastructure across different SSP scenarios. a Change in safety factor. **b** Inequality based on safety factor. **c** Change in the degree of uncertainty. **d** Inequality based on the degree of uncertainty.

exposure, defined as the proportion of affected infrastructure length relative to the total network length within each region. This normalization reduces the influence of infrastructure distribution and highlights spatial variations more directly attributable to hazard intensification. These distinctions suggest that the observed inequalities in adaptation needs are driven by different underlying mechanisms: safety factor disparities are predominantly hazard-driven, whereas exposure-based inequalities reflect both hazard patterns and infrastructure configurations. In this context, the higher safety factors observed in economically constrained regions stem from the spatial coincidence between stronger projected compound precipitation intensification and existing infrastructure systems. Importantly, mitigation pathways reduce both the magnitude of required safety factors and the inequality index across income groups, suggesting that emission reductions may generate co-benefits by moderating adaptation burdens and narrowing resilience gaps. However, scenario-dependent variations in inter-model uncertainty highlight that adaptation planning must account not only for central estimates but also for the spread of model ensembles. The safety factor framework thus serves as a standardized indicator linking climate projections to design-relevant adaptation requirements while revealing underlying inequality in future resilience demands.

This study evaluates the impacts of compound precipitation extremes on global transportation infrastructure primarily from an exposure-based perspective. We acknowledge that engineering design standards and construction codes vary substantially across infrastructure classes and regions. Highways and mainline railways are typically designed to withstand higher return-period events than lower-class roads or branch railways, and design thresholds also differ between developed and developing countries. As a result, identical hazard intensities may correspond to different levels of structural resilience. To ensure global comparability and computational feasibility, we adopted compound precipitation scenarios with 50- and 100-year return periods as standardized hazard benchmarks. These scenarios provide a consistent basis for large-scale assessment but do not explicitly incorporate spatial heterogeneity in engineering capacity. Therefore, the reported inequalities primarily reflect differences in hazard intensity and infrastructure exposure. Future work that integrates spatially explicit information on design standards and adaptive capacity would further improve the accuracy of risk quantification across infrastructure types and regions.

In summary, this study presents a global assessment of inequalities in the impacts of compound precipitation extremes (CPEs) on transportation infrastructure under future climate change. By combining copula-based modeling of joint precipitation extremes with high-resolution multi-model CMIP6 projections and spatially explicit infrastructure data, we quantify both exposure and adaptation requirements using a unified framework. Our results show that CPEs are projected to intensify substantially in the late 21st century, leading to widespread increases in infrastructure exposure. Under SSP585, approximately two-thirds of global transportation infrastructure are projected to face increased exposure risk, with about 12.6 million km experiencing at least a 25% reduction in joint return period. While the largest absolute exposure is concentrated in high-income regions—reaching 4.9 million km compared to 0.6 million km in lower-income regions—adaptation requirements show a clear inverse gradient across income groups. Under SSP585, low-income countries face the highest safety factors for CPEs with a 50-year joint return period (mean of 1.31), followed by lower-middle-income (1.20), upper-middle-income (1.17), and high-income countries (1.15), highlighting a pronounced mismatch between where infrastructure is most exposed and where adaptation needs are greatest. Further, we disentangle the mechanisms underlying these inequalities. Safety factor disparities are primarily driven by spatial heterogeneity in hazard intensification, whereas exposure inequalities reflect the combined effects of hazard changes and infrastructure distribution. The distinction between absolute and relative exposure further highlights that different metrics capture different dimensions of inequality. Mitigation pathways reduce both overall risk and inequality, suggesting that emission reductions can generate co-benefits by alleviating uneven adaptation burdens. However, inter-model uncertainty remains substantial, emphasizing

the need for robust, flexible adaptation strategies. Overall, this study provides a policy-relevant framework linking compound climate extremes to infrastructure design requirements, while revealing embedded global inequalities. These findings underscore the need for integrating hazard dynamics and development patterns into equitable and forward-looking infrastructure adaptation planning[24–26].

Methods

Data

Daily precipitation were obtained from the NASA Earth Exchange Global Daily Downscaled Projections (NEX-GDDP-CMIP6) gridded dataset[27] to generate the compound precipitation extremes (CPEs). The NEX-GDDP-CMIP6 dataset comprises outputs from a total of 25 general circulation models (GCMs). Considering forcing scenarios and data availability, we selected the 11 most widely utilized models (as shown in Supplementary Table S9) in this study, which are deemed sufficient to ensure the robustness of the results[28]. We investigated CPEs in both the historical period (1951–2010) and the future period (2041–2100) under four SSP scenarios (SSP126, SSP245, SSP370, and SSP585).

Open Street Map (OSM) serves as a freely accessible global geographic database comprising roads (https://www.openstreetmap.org/#map=11/22.3558/114.1376), continuously refined and enhanced through the efforts of numerous volunteers[29]. OSM has made significant progress in documenting roads and railways, and has emerged as a leading global resource in this domain, with extensive use in various research endeavors[30,31]. Utilizing OSM's classification system, we identified five major road categories: (1) motorways, (2) trunk roads, (3) primary roads, (4) secondary roads, and (5) tertiary roads. According to OSM definitions: (1) Motorways represent major divided highways with restricted access, typically featuring two or more running lanes alongside an emergency hard shoulder. (2) Trunk roads denote the most crucial roads within a country's network that are not designated as motorways. (3) Primary roads rank next in importance within a country's road system, often serving as connectors between larger towns. (4) Secondary roads follow in importance and frequently connect towns. (5) Tertiary roads come next in importance, often linking smaller towns and villages. Certain minor roads (e.g., footways) are excluded due to uncertainty regarding whether drainage considerations were factored into their construction. Moreover, the largest data gaps within OSM primarily occur in lower-tier roads, such as footways and residential streets. For railways, we include tracks accommodating full-sized passenger or freight trains operating within the standard gauge of each country or region. Road and rail data were obtained from the freely accessible Geofabrik download server, typically refreshed on a daily basis. Our dataset was last updated as of May 6, 2021, and comprises linear vector data featuring spatial positions.

National and subnational boundaries follow the World Bank global administrative map (https://maps.worldbank.org/). This study encompasses 237 countries and territories. For analytical clarity, countries are categorized into income groups based on their 2022 gross national income (GNI) per capita, as calculated by the World Bank Atlas method. Specifically, countries are classified as follows: low-income countries (GNI per capita ≤US$1085), lower-middle-income countries (US$1085 < GNI per capita ≤US$4,255), upper-middle-income countries (US$4255 < GNI per capita ≤US$13,205), and high-income countries (GNI per capita >US $13,205), in accordance with the World Bank's 2022 criteria[32].

Compound precipitation extremes definition

Two extreme precipitation indices, the maximum 1-day precipitation (RX1D) and maximum consecutive 5-day precipitation (RX5D) defined by the Expert Team on Climate Change Detection and Indices (ETCCDI) are used to represent compound precipitation extremes[33–35]. The RX1D and RX5D are widely applied in flood risk assessments. In this study, the simultaneous occurrence of RX1D and RX5D is defined as a compound extreme precipitation event. In this study, we utilize 11 sets of GCM data (with a 0.25° × 0.25°resolution), and each GCM dataset includes 265,274 land grid points globally. For each grid point, we first identify compound extreme events using climate data for the historical periods of 1951–2010 and the future periods of 2041–2100. Subsequently, marginal distributions for RX1D and RX5D are fitted during the historical period, and their joint probability distribution is constructed using a copula function[36], as expressed as follows:

$$u_1 = F_1(x_1|\gamma_1) \tag{1}$$

$$u_2 = F_2(x_2|\gamma_2) \tag{2}$$

where x_1 and x_2 represent RX1D and RX5D; u_1 and u_2 represent the cumulative probability of the RX1D and RX5D;$F_1(x_1|\gamma_1)$ and $F_2(x_2|\gamma_2)$ are marginal distributions of RX1D and RX5D, which are selected from Gumbel, GEV, Gamma, Lognormal, and Weibull distributions. γ_1 and γ_2 are the associated distribution parameters, estimated using the Probability Weighted Moments Estimation (PWME) method (for Extreme Value (Gumbel) and GEV distributions) or the Method of Moments Estimation (MME) (for Gamma and Weibull distributions). The optimal marginal probability distributions are selected based on the minimum Akaike Information Criterion (AIC).

$$F\left(x_1, x_2|\gamma_{1,}, \gamma_2, \theta\right) = C\left[u_1, u_2|\theta\right] \tag{3}$$

where C (.) is a copula function, seleted from the Gaussian, Gumbel, Frank, and Joe Copula functions; θ is the parameter in the copula function that describes the dependence between RX1D and RX5D, estimated using the Maximum Likelihood Estimation (MLE) method. The copula function with the lowest AIC value is chosen as the best-fitting copula. The fitted best marginal distributions and Copula, along with their parameters, will be available on Figshare upon acceptance of the manuscript.

The concept of return period (RP), which describes the long-term average of recurrence interval for one extreme, is one of the most critical indices for hazard risk assessment. When multiple extremes (e.g., RX1D and RX5D etc.) are under consideration, the concept of RP can be extended to the multivariate context, leading to the concept of joint return periods (JRPs). JRPs describe the expected time interval during which all components of the compound extreme exceed the prescribed thresholds. In this study, the JRPs are calculated based on the joint occurrence probability of CPEs under the "AND" condition. For each of the 11 sets of GCM data, we perform the calculation individually. By incorporating future projections of RX1D and RX5D into the fitted marginal distributions and copula function, we obtain the joint return period of CPEs as follows.

$$T^{AND}_{u_1,u_2} = \frac{1}{\Pr(\mathbf{x} \in R^d_{AND})} \tag{4}$$

$$R^d_{AND} = \left\{(\mathrm{x}_1, \mathrm{x}_2) \in R^d : \mathrm{x}_1 > \mathrm{x}^*_1 \bigwedge \mathrm{x}_2 > \mathrm{x}^*_2\right\} \tag{5}$$

Once the interdependence among the attributes of the compound extreme is described by the copula function, the JRPs are able to be reformulated as:

$$T^{AND}_{u_1,u_2} = \frac{1}{\hat{C}(u^*_1, u^*_2|\theta)} \tag{6}$$

where $u^*_i = \Pr(X_i > x^*_i) = 1 - F_i(X^*_i|\gamma_i)$. $\hat{C}$ is the multivariate survival function: $\hat{C}(u) = \bar{C}(1-u)$. More details about the calculation of JRPs are avialibale in our previous research[36,37].

Estimation of the most-likely RX1D and RX5D corresponding to the design joint return period

Another common approach to characterize the hazard scenario for an extreme event is to analyze the system under the most likely compound event among feasible combinations with equal return periods[38]. The essence of the method is to select the multivariate hazard event with the largest joint

probability density[37], which lies on a critical layer corresponding to a given probability level q:

$$x^q = \arg\max f_C(u_1, u_2|\theta) \tag{7}$$

where $f_C(.)$ indicates the density of the copula-based joint probability, $u_1 = F_1(x_1|y_1), u_2 = F_2(x_2|y_2), (x_1, x_2) \in L_q^F$. The critical layer $L^F{}_q$ is defined as:

$$L_q^F = \{(x, y) : Pr((x, y) \in R_{AND}^d) = q\} \tag{8}$$

where R_{AND}^d indicates the indices under consideration which are denoted by the copula function.

Based on the constructed marginal distributions and Copula functions, we utilize sequential quadratic programming (SQP) to determine the intensity of CPEs (i.e., the most-likely RX1D and RX5D) corresponding to the different joint return periods. SQP is an iterative method for constrained nonlinear optimization that can be regarded as a quasi-Newton method[39,40]. In our study, the objective of SQP is to maximize the probability density of CPEs subject to joint return period constraints (e.g., 50- and 100-year). Finally, changes in CPEs and the associated exposure risks of transportation infrastructure are assessed based on two aspects: frequency and intensity.

Estimation of absolute exposure for transportation assets

The absolute exposure is calculated by aggregating all road and railway assets within a grid of ~25 km × 25 km that experience a reduction of over 25% in the CPE's JRP in the future. The absolute exposure is quantified in terms of length. We first calculate the absolute exposure separately for each type of asset (road and railway) in terms of total affected length. These values are then aggregated across all asset types to obtain the total absolute exposure.

$$AE_g = \sum_{i=1}^{n} EL_{g,i} \tag{9}$$

Here, AE_g is the absolute exposure of transportation assets in grid g; i denotes the asset type, with a total of n types; and $EL_{g,i}$ is the absolute exposure length of the ith asset within the grid g.

Estimation of the safety factor for climate change adaptation

The safety factor required for transportation infrastructure, aimed at climate change adaptation with respect to CPEs, is defined as the ratio of the sum of the future most-likely RX1D and RX5D to the sum of historical values with the same JRP, as expressed in Eq. (10)

$$SF_{g,i} = \frac{pre^*_{g,i,1} + pre^*_{g,i,2}}{pre_{g,i,1} + pre_{g,i,2}} \tag{10}$$

Here, $SF_{g,i}$ is the safety factor of the ith asset in the grid g; $pre_{g,i,1}$ and $pre_{g,i,2}$ are the most-likely RX1D and RX5D corresponding to historical CPEs (e.g., with a JRP of 50 years) of the ith asset in grid g; $pre^*_{g,i,1}$ and $pre^*_{g,i,2}$ are the future most-likely RX1D and RX5D corresponding to the same JRP of the ith asset in grid g. A higher safety factor suggests that future CPEs are more intense, implying greater risk to transportation infrastructure and a need for enhanced adaptation measures to improve resilience. Since the estimation of precipitation corresponding to a given JRP is derived from the fitted copula model, the calculated safety factor may be influenced by the choice of copula family. Different copula specifications may lead to variations in the dependence structure between RX1D and RX5D, thereby introducing additional uncertainty into the safety factor estimation. In this study, a commonly used copula family is adopted as a baseline for consistency, while the sensitivity of the results to copula selection is acknowledged as a limitation and an important direction for future research[28,41].

Estimation of uncertainty and inequality

In this study, we further analyzed the uncertainty induced by climate projections, which is reflected in the variance of the safety factor obtained by outputs from 11 CMIP6 models. To account for the uncertainty inherent in these 11 models, we calculated the standard deviation (sd) of these safety factors at each grid point as follows:

$$sd_g = \sqrt{\frac{\sum_{i=1}^{11} (x_i - \bar{x})^2}{10}} \tag{11}$$

Where x_i represents the safety factor calculated based on CPEs data from ith model;

$\bar{x}$ is the mean value.

In addition, the coefficient of variation (sd/mean) was calculated to represent the unequal impacts of CPEs on transportation infrastructure among different income countries under various SSPs in late 21st century

$$\text{Inequality} = \sqrt{\frac{\sum_{i=1}^{4} (z_i - \bar{z})^2}{3}} / \bar{z} \tag{12}$$

Where z_i represents the safety factor for different income countries (i.e., low-income, lower-middle-income, upper-middle-income, and high-income countries), $\bar{z}$ represents the corresponding mean value. The methodological framework of the above analysis is summarized in Supplementary Fig. S9[42].

Data availability

Daily precipitation were obtained from the NASA Earth Exchange Global Daily Downscaled Projections (NEX-GDDP-CMIP6). Transportation infrastructure data were obtained from Open Street Map (OSM). The delineation of national and subnational boundaries adheres to the standard World Bank global administrative map. All the data used in this study will be available on Figshare upon acceptance of the manuscript.

Code availability

All the code used in this study will be available on Figshare upon acceptance of the manuscript.

Received: 20 October 2025; Accepted: 8 May 2026;
Published online: 11 June 2026

References

1. Hallegatte, S., Rentschler, J., & Rozenberg, J. *Lifelines: The Resilient Infrastructure Opportunity* (World Bank Publications, 2019).
2. Koks, E. E. et al. A global multi-hazard risk analysis of road and railway infrastructure assets. *Nat. Commun.* **10**, 2677 (2019).
3. Forzieri, G. et al. Escalating impacts of climate extremes on critical infrastructure in Europe. *Glob. Environ. Change* **48**, 97–107 (2018).
4. ECLAC Irma and Maria by numbers. *Focus ECLAC Caribb.* **1**, 1–18 (2018).
5. Koks, E., Van Ginkel, K., Van Marle, M. & Lemnitzer, A. Brief communication: critical infrastructure impacts of the 2021 mid-July western European flood event. *Nat. Hazards Earth Syst. Sci. Discuss.* **2021**, 1–11 (2021).
6. Verschuur, J. et al. Quantifying climate risks to infrastructure systems: a comparative review of developments across infrastructure sectors. *PLoS Clim.* **3**, e0000331 (2024).
7. Hák, T., Janoušková, S. & Moldan, B. Sustainable development goals: a need for relevant indicators. *Ecol. Indic.* **60**, 565–573 (2016).
8. Liu, K., Wang, Q., Wang, M. & Koks, E. E. Global transportation infrastructure exposure to the change of precipitation in a warmer world. *Nat. Commun.* **14**, 2541 (2023).

9. Martello, M. V. & Whittle, A. J. Estimating coastal flood damage costs to transit infrastructure under future sea level rise. *Commun. Earth Environ.* **4**, 137 (2023).
10. Van Ginkel, K. C., Dottori, F., Alfieri, L., Feyen, L. & Koks, E. E. Flood risk assessment of the European road network. *Nat. Hazards Earth Syst. Sci.* **21**, 1011–1027 (2021).
11. AghaKouchak, A. et al. Climate extremes and compound hazards in a warming world. *Annu. Rev. Earth Planet. Sci.* **48**, 519–548 (2020).
12. Modaresi Rad, A. et al. Human and infrastructure exposure to large wildfires in the United States. *Nat. Sustain.* **6**, 1343–1351 (2023).
13. Verschuur, J., Koks, E. E., Li, S. & Hall, J. W. Multi-hazard risk to global port infrastructure and resulting trade and logistics losses. *Commun. Earth Environ.* **4**, 5 (2023).
14. Kazama, M. & Noda, T. Damage statistics (Summary of the 2011 off the Pacific Coast of Tohoku Earthquake damage). *Soils Found.* **52**, 780–792 (2012).
15. Zhang, Y. & Lam, J. S. L. Estimating the economic losses of port disruption due to extreme wind events. *Ocean Coast. Manag.* **116**, 300–310 (2015).
16. Mühlhofer, E., Koks, E. E., Kropf, C. M., Sansavini, G. & Bresch, D. N. A generalized natural hazard risk modelling framework for infrastructure failure cascades. *Reliab. Eng. Syst. Saf.* **234**, 109194 (2023).
17. Zscheischler, J. et al. Future climate risk from compound events. *Nat. Clim. change* **8**, 469–477 (2018).
18. Ridder, N. N. et al. Global hotspots for the occurrence of compound events. *Nat. Commun.* **11**, 5956 (2020).
19. Mühlhofer, E., Bresch, D. N. & Koks, E. E. Infrastructure failure cascades quintuple risk of storm and flood-induced service disruptions across the globe. *One Earth* **7**, 714–729 (2024).
20. Min, S. K., Zhang, X., Zwiers, F. W. & Hegerl, G. C. Human contribution to more-intense precipitation extremes. *Nature* **470**, 378–381 (2011).
21. Bazai, N. A. et al. Dynamics and impacts of monsoon-induced geological hazards: a 2022 flood study along the Swat River in Pakistan. *Nat. Hazards Earth Syst. Sci.* **25**, 1071–1093 (2025).
22. Wright, D. B., Bosma, C. D. & Lopez-Cantu, T. US hydrologic design standards insufficient due to large increases in frequency of rainfall extremes. *Geophys. Res. Lett.* **46**, 8144–8153 (2019).
23. Liu, K., Wang, M. & Zhou, T. Increasing costs to Chinese railway infrastructure by extreme precipitation in a warmer world. *Transp. Res. Part D Transp. Environ.* **93**, 102797 (2021).
24. Rentschler, J., Salhab, M. & Jafino, B. A. Flood exposure and poverty in 188 countries. *Nat. Commun.* **13**, 3527 (2022).
25. Dasgupta, S., Emmerling, J. & Shayegh, S. Inequality and growth impacts of climate change—insights from South Africa. *Environ. Res. Lett.* **18**, 124005 (2023).
26. Zhang, B., Wang, S., Zscheischler, J. & Moradkhani, H. Higher exposure of poorer people to emerging weather whiplash in a warmer world. *Geophys. Res. Lett.* **50**, e2023GL105640 (2023).
27. Thrasher, B. et al. NASA global daily downscaled projections, CMIP6. *Sci. Data* **9**, 262 (2022).
28. Huang, K. & Fan, Y. R. Parameter uncertainty and sensitivity evaluation of copula-based multivariate hydroclimatic risk assessment. *J. Environ. Inform.* **38**, 131–144 (2021).
29. Map, O. S. Open street map. Acessado em, 12. https://os.openstreetmap.org/ (2014).
30. Meijer, J. R., Huijbregts, M. A., Schotten, K. C. & Schipper, A. M. Global patterns of current and future road infrastructure. *Environ. Res. Lett.* **13**, 064006 (2018).
31. Mooney, P., & Minghini, M. A review of OpenStreetMap data. In *Mapping and the Citizen Sensor*, 37–59 (Ubiquity press, 2017).
32. New World Bank country classifications by income level: 2022-2023. https://blogs.worldbank.org/opendata/new-world-bank-country-classifications-income-level-2022-2023 (2024).
33. Tegegne, G., Melesse, A. M. & Alamirew, T. Projected changes in extreme precipitation indices from CORDEX simulations over Ethiopia, East Africa. *Atmos. Res.* **247**, 105156 (2021).
34. Li, H., Chen, H., Wang, H. & Yu, E. Future precipitation changes over China under 1.5 C and 2.0 C global warming targets by using CORDEX regional climate models. *Sci. Total Environ.* **640**, 543–554 (2018).
35. Karl, T. R., Nicholls, N. & Ghazi, A. In Weather and Climate Extremes: Changes, Variations and A Perspective from the Insurance Industry. *Clivar/GCOS/WMO workshop on indices and indicators for climate extremes workshop summary.* 3–7 (1999).
36. Fan, Y. R., Yu, L., Shi, X. & Duan, Q. Y. Tracing uncertainty contributors in the multi-hazard risk analysis for compound extremes. *Earths Future* **9**, e2021EF002280 (2021).
37. Fan, Y., Yu, L. & Shi, X. Uncertainty quantification and partition for multivariate risk inferences through a factorial multimodel Bayesian copula (FMBC) system. *J. Hydrol.* **598**, 126406 (2021).
38. Sadegh, M. et al. Multihazard scenarios for analysis of compound extreme events. *Geophys. Res. Lett.* **45**, 5470–5480 (2018).
39. Bonnans, J. F., Gilbert, J. C., Lemaréchal, C., & Sagastizábal, C. A. *Numerical Optimization: Theoretical and Practical Aspects* (Springer Science & Business Media, 2006).
40. Kraft, D. A software package for sequential quadratic programming. Forschungsbericht- Deutsche Forschungs- und Versuchsanstalt fur Luft- und Raumfahrt (1988).
41. Fan, Y., Huang, K., Huang, G., Li, Y. & Wang, F. An uncertainty partition approach for inferring interactive hydrologic risks. *Hydrol. Earth Syst. Sci.* **24**, 4601–4624 (2020).
42. Guo, J. et al. Rising compound hot-dry extremes engendering more inequality in human exposure risks. *npj Nat. Hazards* **2**, 66 (2025).

Acknowledgements

This research was supported by the Natural Science Foundation (52509001), the China Postdoctoral Science Foundation-funded project (2023M730282, GZB20230069), the Academy of Medical Sciences, British Academy, Royal Academy of Engineering, Royal Society and the International Science Partnerships Fund (NGR2\1867).

Author contributions

Writing-review and editing: F.W., Y.F., G.H., and A.A. Experimental operation: J.G., Y.W., and F.W. Data acquisition and validation: J.G., and F.W. Funding acquisition: Y.L., Z.S., Y.Z. All authors reviewed the manuscript.

Competing interests

The authors declare no competing interests.

Additional information

Supplementary information The online version contains supplementary material available at https://doi.org/10.1038/s44304-026-00225-4.

Correspondence and requests for materials should be addressed to Yurui Fan.

Reprints and permissions information is available at http://www.nature.com/reprints

Publisher's note Springer Nature remains neutral with regard to jurisdictional claims in published maps and institutional affiliations.

Open Access This article is licensed under a Creative Commons Attribution 4.0 International License, which permits use, sharing, adaptation, distribution and reproduction in any medium or format, as long as you give appropriate credit to the original author(s) and the source, provide a link to the Creative Commons licence, and indicate if changes were made. The images or other third party material in this article are included in the article's Creative Commons licence, unless indicated otherwise in a credit line to the material. If material is not included in the article's Creative Commons licence and your intended use is not permitted by statutory regulation or exceeds the permitted use, you will need to obtain permission directly from the copyright holder. To view a copy of this licence, visit http://creativecommons.org/licenses/by/4.0/.

© The Author(s) 2026